BMI-1 Modulation and Trafficking During M Phase in Diffuse Intrinsic Pontine Glioma

Banlanjo Umaru[1#], Deepak Kumar Mishra[1,2#], Shiva Senthil Kumar[1], Hao-Han Pang[1,3], Brendan Devine[1], Komal Khan[1], and Rachid Drissi[1,4*]

[1]Center for Childhood Cancer Research, Nationwide Children's Hospital, Columbus, OH, USA
[2]Colket Translational Research, Department of Pediatrics, Children's Hospital of Philadelphia, PA, USA
[3]Center for Drug Research and Development, College of Human Ecology, Chang Gung University of Science and Technology, Taoyuan, Taiwan
[4]The Ohio State University College of Medicine, Columbus, OH, USA

[2,3]Present address
[#]Contributed equally to this work

[*]**Corresponding Author:** Rachid Drissi, Center for Childhood Cancer Research, Nationwide Children's Hospital, 575 Children's Crossroad, Columbus, OH, USA; Phone: 614-355-3749; Fax: 614-355-2927; Email: Rachid.Drissi@nationwidechildrens.org

Summary:

BMI-1 (B cell-specific Moloney murine leukemia virus integration site 1) has been implicated in both normal and cancer cell biology. While the canonical function of BMI-1 involves epigenetic repression, novel extra-nuclear functions have been recently reported. In the present study, we demonstrate that the phosphorylation of BMI-1 in diffuse intrinsic pontine glioma (DIPG) cells occurs in M phase and that triggers simultaneous translocation of the phosphorylated BMI-1 to the cytoplasm. This translocation is mediated by the RanGTP-dependent transporter CRM1, also known as exportin. Furthermore, we uncovered a previously unidentified nuclear export signal (NES) in BMI-1 protein, suggesting an active transport type of modified BMI-1 mediated by CRM1. These findings associate BMI-1 phosphorylation with its trafficking in M phase. Collectively, this study sheds light on the molecular mechanisms underlying BMI-1 functions in DIPG, thereby potentially paving the way for the development of targeted therapeutic strategies related to M phase progression.

Keywords: BMI-1, phosphorylation, cell cycle, NES, DIPG

Introduction

BMI-1 is a highly conserved protein initially identified as a proto-oncogene that cooperates with c-MYC in the tumorigenesis of murine B-cell lymphoma [1]. It is a subunit of the Polycomb repressive complex 1 (PRC1) required for the canonical RING1B mediated E3-ubiquitin ligase activity that catalyzes the ubiquitination of histone H2A at lysine 119 (H2A-K119Ub). BMI-1-associated E3 ubiquitin ligase activity represses multiple gene loci, including *INK4A/ARF* locus encoding for two tumor suppressors $p16^{INK4A}$ and $p14^{ARF}$ [2]. BMI-1 has been implicated in a number of biological functions including development, cell cycle, DNA damage response (DDR), senescence, stem cell self-renewal and differentiation [3]. Furthermore, BMI-1 is highly expressed in multiple malignancies and is involved in therapy resistance, tumorigenesis, metastasis, and cancer recurrence[3,4]. These functions are attributed to three domains of BMI-1; the N-terminal RING finger (RF) and the central helix-turn-helix (HTH) domains that are responsible for its interaction with DNA thereby facilitating gene repression, DDR and senescence prevention [5-8]. The C-terminal PEST domain harbors several phosphorylation sites and confers protein stability and increased oncogenic potential in multiple cancers[9-12]. Additionally, BMI-1 contains two nuclear localization sequences (NLS1 and NLS2), with only NLS2 shown to be responsible for its nuclear localization[13,14].

BMI-1 is tightly regulated both at the transcriptional and the post-translational level. While transcriptional regulation has been extensively studied, the role of post-translational modifications in modulating BMI-1 function is poorly understood[15]. Recent reports have elucidated novel non-nuclear functions of BMI-1. For example, BMI-1 has been shown to localize to the inner mitochondrial membrane supporting the stability of mitochondrial RNA transcripts and thereby regulates mitochondrial function[14,16]. BMI-1 has also been shown to regulate the expression of androgen receptor in prostate cancer, through direct binding in a PRC1-independent manner[17,18]. In support of these extra-nuclear functions, BMI-1 has been previously shown to be associated with chromatin when hypo-phosphorylated in G_1/S, and dissociates from the chromatin in M phase

when phosphorylated[19]. Recently, we showed cytoplasmic translocation of phosphorylated BMI-1 in M phase [20]. However, the process of BMI-1 translocation from the nucleus to the cytoplasm and its role during M phase remain largely unknown. In the current study, we show that the cytoplasmic translocation of BMI-1 is M phase specific and PRC1-independent. This translocation is an active process mediated by exportin (CRM-1). Additionally, we have identified a novel nuclear export signal (NES) sequence within the BMI-1 protein that allows transport to the cytoplasm by CRM1.

Results

Phosphorylated BMI-1 is translocated to the cytoplasm in M phase

In our previous studies with PTC596, a mitotic blocker, we showed that treatment with PTC596 led to BMI-1 phosphorylation and this modification correlated with its translocation to the cytoplasm in cells arrested in M phase [20]. To confirm these observations, we synchronized CCHMC-DIPG-1 cells in M phase using nocodazole (Figure 1A) and observed time-dependent accumulation of phosphorylated BMI-1 as the cells arrested in M phase (Figure 1B). Using previously established mitotic blockers, colchicine or PTC596, we observed an accumulation of phosphorylated BMI-1 in the cytoplasmic compartment in cells arrested in M phase (Figures 1C and 1D). Moreover, these observations were further validated in cell synchronization studies using PTC596 (Figures S1A-C). Using another DIPG cell line (SU-DIPG-IV) treated with either PTC596 or colchicine as well as with λ-phosphatase, we showed that modification of BMI-1 occurs via phosphorylation (Figure S1D). Of note, we used Cyclin B1 as a surrogate marker for identifying cells in the G_2/M phase in both immunoblot and immunofluorescence (IF) assays. Consistent with previous findings, Cyclin B1 accumulates in the cytoplasm as cells approached prophase[21-23].

Given that BMI-1 is a crucial component of the PCR1 complex, we aimed to investigate whether its phosphorylation and translocation influence the trafficking of the entire complex. Interestingly,

RING1B, the catalytic subunit of PRC1 complex, was not translocated to the cytoplasm when treated with PTC596 or colchicine (Figure 1E). Furthermore, IF analysis validated these findings by confirming cytoplasmic translocation of BMI-1 and not of RING1B (Figures 1F and 1G) in M phase cells as evidenced by H3 S10-P positive staining. Together these data suggest that BMI-1 phosphorylation and translocation to the cytoplasm in M phase is PRC1-independent.

Transport of modified BMI-1 to the cytoplasm is CRM1 dependent.

When treated with PTC596, we observed a small percentage of cells showing both cytoplasmic and nuclear BMI-1 distribution (Figure S2A), suggesting that BMI-1 may be actively transported from the nucleus to the cytoplasm during M phase. Nuclear export of majority of proteins to the cytoplasm are directed by the nuclear export receptor CRM1 or exportin-1[24,25]. Leptomycin-B (LMB), a potent selective inhibitor of CRM1-mediated transport, has been previously reported to inhibit nuclear export of Cyclin B1 in a time-dependent manner[21,26]. We observed a gradual decrease in cytoplasmic BMI-1 and a consequent increase in the nuclear levels in a time-dependent manner when treated with LMB (Figure 2A). Interestingly, when treated together with PTC596, LMB inhibited the cytoplasmic translocation of phosphorylated BMI-1 in M phase (Figures 2B and D). Moreover, LMB treatment interfered with PTC596-induced M phase arrest (Figure 2C). Together, these data suggest that the BMI-1 translocation to the cytoplasm in M phase is an active process and is CRM1-dependent.

Characterization of functional NES motif in BMI-1

CRM1 mediated transport requires a leucine-rich sequence in the target cargo proteins that have been characterized as nuclear export signals (NES)[27,28]. Using an NES prediction pipeline [29], we identified a previously unidentified putative NES sequence, 175-LRKFLRSKMDI-185 within HTH

domain (Figure S3A). This sequence conforms to the NES consensus Class 1C sequence (φ-XXX-φ-XXX-φ-X-φ)[30,31] and is highly conserved across multiple species (Figures 3A and B). Additionally, mutations in the *CRM1* gene has been previously shown to interfere with the transport function of the CRM1 protein[32]. We confirmed that CCHMC-DIPG-1 cells do not harbor any mutations in the *CRM1* gene. To examine whether the putative NES sequence is functional, we ectopically expressed ΔNES-BMI-1 (D1- ΔNES-BMI-1) as well as the BMI-1 overexpression control (D1-BMI-1) in CCHMC-DIPG-1 cells (Figure S3B). When treated with PTC596, we observed both a decrease in phosphorylation in D1-ΔNES-BMI-1, and a defect in phosphorylated BMI-1 cytoplasmic translocation compared to D1-BMI-1. Importantly, the ectopic expression of ΔNES-BMI-1 did not affect the phosphorylation and cytoplasmic translocation of endogenous BMI-1 (Figures 3C and S3A). Moreover, the ectopic expression of ΔNES-BMI-1 did not affect the M phase arrest of cells treated with PTC596 (Figures 3C and D), suggesting that a novel NES sequence identified in BMI-1 may be specifically involved in conformational change and translocation of phosphorylated BMI-1 in M phase.

Discussion

Diffuse Intrinsic Pontine Glioma (DIPG) represents one of the most aggressive malignancies of the central nervous system, predominantly affecting children with a median overall survival of less than one year. Hence, there is an urgent need to develop novel therapies that not only improve outcome but mitigate long-term complications in children with DIPG. We have previously identified BMI-1 as a potential therapeutic target in DIPG and have shown that BMI-1 is highly expressed in DIPG tumors regardless of DIPG subtype[33]. The protein BMI-1, a critical component of the Polycomb Repressive Complex 1 (PRC1), is a proto-oncogene implicated in development, stemness of normal and malignant cells, and self-renewal. Elucidating the molecular mechanisms

underlying BMI-1 functions in DIPG-M phase progression will contribute to the development of targeted therapeutic strategies.

We have previously reported the phosphorylation of BMI-1 in M phase and the simultaneous translocation to the cytoplasm of modified BMI-1 when DIPG cells were treated with PTC596[20]. Our present study demonstrates that the phosphorylation and translocation of BMI-1 is independent of the PRC1 complex. Interestingly, the translocation is an active process mediated by CRM1, an essential mediator of nuclear protein export. Voncken *et al.* using osteosarcoma cells, showed that BMI-1 was phosphorylated at the G_2/M phase of the cell cycle and dissociates with PRC1 complex proteins from chromatin[34,35]. However, in this study, we observed colocalization of RING1B, the catalytic subunit of the PRC1 complex, with chromatin and no cytoplasmic translocation during M-phase in our DIPG cells treated either with colchicine or PTC596 (Figures 1E and 1F). This suggests that the phosphorylation and translocation to the cytoplasm of BMI-1 is PRC1-independent and indicate a non-canonical role of BMI-1 in DIPG cells. Moreover, we have previously demonstrated high expression levels of BMI-1 and normal levels of RING1B in DIPG tumor tissues in all subtypes of patient-derived DIPG neurospheres[33], suggesting extranuclear PRC1-independent and non-canonical functions of BMI-1. Further studies are required to elucidate these extranuclear functions of phosphorylated BMI-1 in DIPG. Extranuclear BMI-1 has been shown to localize to the inner mitochondrial membrane to stabilize the mitochondrial RNA, thereby regulating the electron transport chain, which enhances oxidative phosphorylation and ATP synthesis and prevents aberrant ROS production[36,37].

During mitosis, the RanGTPases, including CRM1, control multiple cellular processes involving nuclear transport, mitotic checkpoints, spindle assembly, and post-mitotic nuclear envelope reassembly[24,25]. Here, we show that phosphorylated BMI-1 is transported actively from the nucleus to the cytoplasm via CRM1. A comprehensive analysis of the mitosis events is required to determine the timing of BMI-1 phosphorylation and consequent transport from the nucleus to the cytoplasm during M phase. We have previously postulated that BMI-1 phosphorylation occurs

in early metaphase before induction of the spindle assembly checkpoint (SAC) and the anaphase promoting complex (APC/C^{CDC20})[20], albeit Kim *et al.* have suggested that PTC596 directly inhibits the APC/C^{CDC20} leading to persistent cyclin-dependent kinase (CDK)1/2 activity and BMI-1 hyper-phosphorylation, as well as reduced PRC1 activity[38]. In this study, we identified for the first time an NES sequence in BMI-1 protein involved in its CRM1-mediated nuclear export. Indeed, previous studies have reported an NES-dependent nuclear export of Cyclin B1 by CRM1[21-23]. Moreover, treatment with LMB, which was shown to inhibit interactions of CRM1 with NES[39], coupled with Cyclin B1 accumulation in the nucleus led to cell cycle arrest in S and G2[21]. Furthermore, LMB inhibition of CRM1 was shown to disrupt mitotic progression and chromosome segregation[40]. As expected, we observed an inhibition of PTC596 induced M phase arrest when cells were treated with LMB thus interfering with modified BMI-1 translocation. Several questions remain to be answered to elucidate the exact role of BMI-1 phosphorylation in tumor progression. We are currently performing further studies to determine the phosphorylation sites, upstream kinases, effects of phosphorylation on structural modification of BMI-1, new binding partners of modified BMI-1, and ultimately the extranuclear locations and non-canonical functions of BMI-1. Finally, our results are indicative of a non-canonical role of BMI-1 in DIPG during M phase.

Limitations of the study

Here, we showed that overexpression of GFP-tagged BMI-1 with truncated NES (D1-ΔNES-BMI-1) in CCHMC-DIPG1 cells leads to defects in both BMI-1 phosphorylation and cytoplasmic translocation. However, CCHMC-DIPG-1 cells have high endogenous BMI-1 expression that might interfere with the overexpression of ΔNES-BMI-1. Our future experiments will include an inducible knockout of endogenous BMI-1 to study the role of NES in BMI-1 phosphorylation and translocation. Although we optimized the treatment timepoints, we cannot rule out a potential LMB

interference with the cell cycle progression. Future studies including site directed mutagenesis of Lysine residues in the NES domain should elucidate its role in BMI-1 transport.

Resource availability

Lead contact

Further information and requests for resources and reagents should be directed to and will be fulfilled by the lead contact, Rachid Drissi (Rachid.Drissi@nationwidechildrens.org).

Materials availability

This study did not generate new unique reagents.

Data and code availability

This paper does not report original code. Scripts and code utilized in this study are available from the lead contact upon request.

Acknowledgements

This work was supported by the Department of Defense grant 13709017, the National Center for Advancing Translational Sciences grant UM1TR004548, PTC Therapeutics, Inc. and Nationwide Children's Hospital, Columbus, OH. We thank M. Monje (Stanford University) for kindly providing us with SU-DIPG-IV cells. We thank PTC Therapeutics, Inc. for providing PTC596.

Author contributions

Conception and design: D.K.M, B.U., S.S.K., H-H.P., and R.D.
Development of methodology: D.K.M., S.S.K., B.U., H-H.P., and R.D.
Acquisition of data: D.K.M., S.S.K., B.D., and U.B.
Analysis and interpretation of data: D.K.M., S.S.K., B.U., and R.D.
Writing, review, and/or revision of the manuscript: all authors.
Administrative, technical, or material support: B.D., and K.K.
Study supervision: R.D.

Declaration of interests

The authors declare no competing interests.

STAR ★ methods

Key resources table

REAGENT or RESOURCE	SOURCE	IDENTIFIER
Antibodies		
BMI-1 (D42B3) Rabbit mAb	Cell signaling	Cat# 5856, RRID: AB_10838137
BMI-1 (D20B7) XP® Rabbit mAb	Cell signaling	Cat# 6964, RRID: AB_10828713
RING1B (D22F2) XP® Rabbit mAb	Cell signaling	Cat# 5694, RRID: AB_10705604
Ubiquityl-Histone H2A (Lys119) (D27C4) XP Rabbit mAb	Cell signaling	Cat# 8240S, RRID: AB_10891618
Phospho-Histone H3 (Ser10) (6G3) Mouse mAb	Cell signaling	Cat# 9706, RRID: AB_331748
Cyclin B1 Antibody Rabbit pAb	Cell signaling	Cat# 4138, RRID: AB_2072132
Cleaved Caspase-3 (Asp175) Antibody Rabbit pAb	Cell signaling	Cat# 9661, RRID: AB_2341188
Histone H3 (96C10) Mouse mAb	Cell signaling	Cat# 3638S, RRID: AB_1642229
Histone H2A (L88A6) Mouse mAb	Cell signaling	Cat# 3636, RRID: AB_2118801
β-Actin (8H10D10) Mouse mAb	Cell signaling	Cat# 3700, RRID: AB_2242334
Alexa Fluor® 488 AffiniPure™ Donkey Anti-Rabbit IgG (H+L)	Jackson ImmunoResearch	Cat# 711-545-152, RRID: AB_2313584
Alexa Fluor® 594 AffiniPure™ Donkey Anti-Mouse IgG (H+L)	Jackson ImmunoResearch	Cat# 715-585-150, RRID: AB_2340854
Goat anti-mouse IgG (H+L) Secondary Antibody, HRP	Thermo Fisher Scientific	Cat# 31430, RRID: AB_228307
Goat anti-Rabbit IgG (H+L) Secondary Antibody, HRP	Thermo Fisher Scientific	Cat# 31460, RRID: AB_228341
Cell lines		
SU-DIPG-IV	M. Monje (Stanford University)	N/A
CCHMC-DIPG-1	Lab generated	N/A
HEK293T	ATCC	RRID: CVCL_0063
Plasmids		
pLVX-AcGFP1-N1 Vector	Clontech	#632154
pMDLg/pRRE	Addgene	#12251, RRID: Addgene_12251
pMD2.G	Addgene	#12259, RRID: Addgene_12259
pRSV-Rev	Addgene	#12253, RRID: Addgene_12253
Chemicals		
Thymidine	Sigma	CAS# 50-89-5

Nocodazole	Sigma	CAS# 31430-18-9
PTC596	PTC Therapeutics	N/A
λ-Phosphatase	NEB	Cat# P0753S
DAPI	Vector Laboratories	H1200
Colchicine	Sigma	CAS# 64-86-8
Leptomycin-B	Sigma	CAS# 87081-35-4
Commercial kits		
Universal Mycoplasma Detection Kit	ATCC	30-1012K ™
Software		
FlowJo v.10	FlowJo, USA	https://www.flowjo.com
Image Studio Lite	LI-COR	https://www.licorbio.com/image-studio-lite
GraphPad Prism 8.0.1	GraphPad software	https://www.graphpad.com/scientific-software/prism/
Image J	NIH image	https://imagej.net/ij/index.html

Experimental model and subject details

Cell lines

The primary patient-derived DIPG cells SU-DIPG-IV and CCHMC-DIPG-1 were cultured as previously described [20]. SU-DIPG-IV was authenticated by our collaborator M. Monje (Stanford University). CCHMC-DIPG-1 cells were generated and authenticated by the Drissi laboratory. Using the Universal Mycoplasma Detection Kit (ATCC; 30-1012K) all cell lines used in this study were confirmed to be negative for mycoplasma contamination**.** HEK293T cells (ATCC, RRID: CVCL_0063) were purchased from ATCC and used for lentiviral vector packaging.

Reagents

Thymidine (Sigma, CAS# 50-89-5), Colchicine (Sigma CAS# 64-86-8), Leptomycin-B (Sigma CAS# 87081-35-4) and Nocodazole (Sigma CAS# 31430-18-9) was reconstituted in sterile water. PTC596 was provided by PTC Therapeutics (South Plainfield, NJ, USA) and was reconstituted in DMSO for *in vitro* studies.

Method details

Generation of ΔNES-BMI-1 mutants

The NES deletion (ΔNES-BMI-1) cDNA was generated through overlap extension PCR. Wild type (WT) and the NES deletion (ΔNES) BMI-1 cDNA were cloned into pLVX-AcGFP1-N1 Vector (Clontech, #632154) to create GFP-tagged expression vectors. These vectors were transfected into HEK293T cells with additional helper plasmids pMDLg/pRRE (#12251), pMD2.G (#12259), pRSV-Rev (#12253) from Addgene. Supernatant containing viruses were collected 48 hours post-transfection, concentrated and directly added to CCHMC-DIPG-1 cells. GFP positive cells were sorted and expanded. NES deletion was confirmed through Sanger sequencing.

Cell Cycle, Proliferation and Apoptosis Assays

Cell cycle was analyzed as previously described[20]. Data were analyzed using FlowJo v.10 (FlowJo, USA) software. Cell proliferation was measured using WST-1 assay (Takara Bio, MK400) as per manufacturer's instructions. WST-1 reagent was added to each well at a final concentration of 1:10, incubated for 1.5 hour at 37°C, and absorbance was measured at 450 nm with 650 nm as the reference wavelength.

Western Blotting

Immunoblot assays were performed as previously described[20]. Antibodies used were against BMI-1 (Cell signaling, Cat# 5856, RRID: AB_10838137, 1:1000), H2AK119Ub (Cell signaling, Cat# 8240S, RRID: AB_10891618, 1:1000), H3 S10-P (Cell signaling, Cat# 9706, RRID: AB_331748, 1:1000), Cyclin B1 (Cell signaling, Cat# 4138, RRID: AB_2072132, 1:1000), Cleaved caspase-3 (Cell signaling Cat# 9661, RRID: AB_2341188, 1:1000), Total Histon H3 (Cell signaling Cat# 3638S, RRID: AB_1642229, 1:1000), Total Histon H2A (Cell signaling Cat# 3636, RRID: AB_2118801, 1:1000), β-Actin (Cell signaling Cat# 3700, RRID: AB_2242334, 1:1000).

Membranes were stained with corresponding secondary antibodies, Goat anti-mouse IgG (H+L) Secondary Antibody, HRP (Thermo Fisher Scientific, Cat# 31430, RRID: AB_228307, 1:1000) or Goat anti-Rabbit IgG (H+L) Secondary Antibody, HRP (Thermo Fisher Scientific, Cat# 31460, RRID: AB_228341, 1:1000). Bands visualized with ECL were captured using Azurec500 imaging system (Azure Biosystems) and quantified using Image Studio Lite (LI-COR). For the λ-Phosphatase experiments, 15 µg of protein lysates were treated with λ-Phosphatase (NEB, Cat# P0753S) according to manufacturer's protocol and then immunoblot was performed. Cytoplasmic and nuclear fractions were isolated as described elsewhere [41].

Immunofluorescence (IF)

Immunostaining was performed as described previously [20]. Primary antibodies were used against BMI-1 (Cell signaling, Cat# 6964, RRID: AB_10828713, 1:500), RING1B (Cell signaling, Cat# 5694, RRID: AB_10705604, 1:500), H3 S10-P (Cell signaling, Cat# 9706, RRID: AB_331748, 1:500), Cyclin B1 (Cell signaling, Cat# 4138, RRID: AB_2072132, 1:500) were stained with corresponding secondary antibodies, Alexa Fluor® 488 AffiniPure™ Donkey Anti-Rabbit IgG (H+L) (Jackson ImmunoResearch, Cat# 711-545-152, RRID: AB_2313584, 1:500) or Alexa Fluor® 594 AffiniPure™ Donkey Anti-Mouse IgG (H+L) (Jackson ImmunoResearch, Cat# 715-585-150, RRID: AB_2340854, 1:500). For nuclear staining, cells were embedded with mounting media with DAPI (Vector Laboratories, H1200). Images were captured with 60 X oil objective on Nikon Eclipse Ti confocal microscope. Quantifications were performed using ImageJ software (NIH image).

Quantification and statistical analysis

Data from at least two independent experiments with individual technical replicates wherever applicable were collected. Representative images or blots are shown. Results are shown as mean ± SD. GraphPad Prism 8.0.1 was used to perform statistical analysis. One- or Two-way ANOVA

followed by a post-hoc Dunnet's or Tukey test, wherever applicable, was used to analyze the data.

Supplemental information

PDF Document included. Figures S1–S3

Figure Legends

Figure 1. Phosphorylation and translocation of BMI-1 occurs in M phase

(**A)** Scheme for the cell synchronization studies (top) and corresponding cell cycle analysis by flow cytometry (bottom). The percentage of cells in each cell cycle is indicated.

(**B)** Immunoblot analysis of BMI-1 at the indicated timepoints. The arrow indicates phosphorylated BMI-1. β-Actin is used as the loading control.

(**C)** Immunoblot analysis of BMI-1, Cyclin B1 and histone H3 S10-P in the cytoplasmic (C) and nuclear (N) fractions when treated with PTC596 (100 nM for 24 h) or colchicine (100 ng/ml for 24 h). β-Actin and total H3 served as loading controls. Arrow indicates phosphorylated BMI-1.

(**D)** Representative immunofluorescence images showing DAPI (blue), Cyclin B1 (green) and BMI-1 (red) in cells treated with PTC596 or colchicine at the indicated doses for 24 h. White arrows indicate the cells with cytoplasmic localization of BMI-1.

(**E)** immunoblot analysis of RING1B in the cytoplasmic (C) and nuclear (N) fractions in cells treated with PTC596 (100 nM for 24h) or colchicine (100 ng/ml for 24h).

(**F)** Representative immunofluorescence images showing DAPI (blue), H3-S10-P (green) and RING1B (red) in cells treated with 100 nM PTC596 for 24 h. White arrows indicate the cells with cytoplasmic localization of BMI-1.

(G) Representative immunofluorescence images showing DAPI (blue), H3-S10-P (green) and RING1B (red) in cells treated with 100 nM PTC596 for 24 h. Yellow arrows indicate the cells with RING1B still localized within DNA.

All experiments were conducted in CCHMC-DIPG-1 cells at n=2.

P values are indicated (*, P < 0.05; ns, not significant (P>0.05))

Figure 2. M phase translocation of BMI-1 is an active process

(A) Immunoblot analysis of BMI-1, Cyclin B1 and H3 S10-P in the cytoplasmic and nuclear fractions of cells treated with leptomycin B (LMB) for the indicated time points. β-Actin and total H3 served as the loading controls.

(B) Scheme for the combination experiment of LMB with PTC596 (top) and corresponding immunoblot analysis of BMI-1 and H3 S10-P in the cytoplasmic and nuclear fractions (bottom). β-Actin and total H3 served as loading controls.

(**C)** Cell cycle analysis by flow cytometry of cells treated with LMB and PTC596. The percentage of cells in each cell cycle phase is indicated.

(D) Representative immunofluorescence images showing DAPI (blue), BMI-1 (green) and H3 S10-P (red) in cells treated with PTC596 and LMB based on scheme in **(B).** White arrows indicate the cells with cytoplasmic localization of BMI-1. All experiments were conducted in CCHMC-DIPG-1 cells at n=2.

P values are indicated (*, P < 0.05)

Figure 3. Identification and characterization of NES in BMI-1.

(A) Output of the NES prediction pipeline NetNES 1.1 showing putative NES signals in the BMI-1 protein sequence (NN = neural network algorithm; HMM = hidden Markov Model algorithm; NES score = combination of NN and HMM algorithms). A signal above the threshold signifies a highly probable NES hit.

(B) Alignment of the identified BMI-1 NES sequence in multiple species, verified NES sequences in TERT and SNUPN and the NES consensus sequences showing high homology.

(**C)** Immunoblot analysis of BMI-1, H3 S10-P from cytoplasmic (C) and nuclear (N) fractions of D1-BMI-1 and D1-ΔNES-BMI-1 cells treated with PTC596. β-Actin and total H3 served as loading controls. BMI-1-GFP is ectopically expressed in D1-BMI-1 and D1-ΔNES-BMI-1. Arrows indicate phosphorylated BMI-1.

(**D)** Cell cycle analysis by flow cytometry of cells of D1-WT-BMI-1 and D1-ΔNES-BMI-1 cells treated with DMSO or PTC596 (100 nM for 24h). The percentage of cells in each cell cycle phase is indicated.

References

1 van Lohuizen, M. *et al.* Identification of cooperating oncogenes in E mu-myc transgenic mice by provirus tagging. *Cell* **65**, 737-752 (1991).

2 Jacobs, J. J. *et al.* Bmi-1 collaborates with c-Myc in tumorigenesis by inhibiting c-Myc-induced apoptosis via INK4a/ARF. *Genes & development* **13**, 2678-2690 (1999).

3 Bhattacharya, R., Mustafi, S. B., Street, M., Dey, A. & Dwivedi, S. K. Bmi-1: At the crossroads of physiological and pathological biology. *Genes Dis* **2**, 225-239 (2015). https://doi.org/10.1016/j.gendis.2015.04.001

4 Sahasrabuddhe, A. A. BMI1: A Biomarker of Hematologic Malignancies. *Biomark Cancer* **8**, 65-75 (2016). https://doi.org/10.4137/bic.S33376

5 Facchino, S., Abdouh, M., Chatoo, W. & Bernier, G. BMI1 confers radioresistance to normal and cancerous neural stem cells through recruitment of the DNA damage response machinery. *The Journal of neuroscience : the official journal of the Society for Neuroscience* **30**, 10096-10111 (2010). https://doi.org/10.1523/JNEUROSCI.1634-10.2010

6 Ginjala, V. *et al.* BMI1 Is Recruited to DNA Breaks and Contributes to DNA Damage-Induced H2A Ubiquitination and Repair. *Molecular and Cellular Biology* **31**, 1972-1982 (2011). https://doi.org/10.1128/MCB.00981-10

7 Ismail, I. H., Andrin, C., McDonald, D. & Hendzel, M. J. BMI1-mediated histone ubiquitylation promotes DNA double-strand break repair. *The Journal of cell biology* **191**, 45-60 (2010). https://doi.org/10.1083/jcb.201003034

8 Itahana, K. *et al.* Control of the replicative life span of human fibroblasts by p16 and the polycomb protein Bmi-1. *Mol Cell Biol* **23**, 389-401 (2003). https://doi.org/10.1128/mcb.23.1.389-401.2003

9 Kim, J., Hwangbo, J. & Wong, P. K. Y. p38 MAPK-Mediated Bmi-1 Down-Regulation and Defective Proliferation in ATM-Deficient Neural Stem Cells Can Be Restored by Akt Activation. *PLoS ONE* **6**, e16615-e16615 (2011). https://doi.org/10.1371/journal.pone.0016615

10 Liu, Y. *et al.* Akt phosphorylates the transcriptional repressor Bmi1 to block its effects on the tumor-suppressing Ink4a-Arf locus. *Science Signaling* **5**, ra77-ra77 (2012). https://doi.org/10.1126/scisignal.2003199
11 Nacerddine, K. *et al.* Akt-mediated phosphorylation of Bmi1 modulates its oncogenic potential, E3 ligase activity, and DNA damage repair activity in mouse prostate cancer. *Journal of Clinical Investigation* **122**, 1920-1932 (2012). https://doi.org/10.1172/JCI57477
12 Yadav, A. K. *et al.* Deletion analysis of BMI1 oncoprotein identifies its negative regulatory domain. *Molecular Cancer* **9**, 158 (2010). https://doi.org/10.1186/1476-4598-9-158
13 Cohen, K. J., Hanna, J. S., Prescott, J. E. & Dang, C. V. Transformation by the Bmi-1 oncoprotein correlates with its subnuclear localization but not its transcriptional suppression activity. *Molecular and Cellular Biology* **16**, 5527-5535 (1996). https://doi.org/doi:10.1128/MCB.16.10.5527
14 Mustafi, S. B. *et al.* Mitochondrial BMI1 maintains bioenergetic homeostasis in cells. *The FASEB Journal* **30**, 4042-4055 (2016). https://doi.org/10.1096/fj.201600321r
15 Bhattacharya, R., Mustafi, S. B., Street, M., Dey, A. & Dwivedi, S. K. D. Bmi-1: At the crossroads of physiological and pathological biology. *Genes & Diseases* **2**, 225-239 (2015). https://doi.org/10.1016/j.gendis.2015.04.001
16 Liu, J. *et al.* Bmi1 regulates mitochondrial function and the DNA damage response pathway. *Nature* **459**, 387-392 (2009). https://doi.org/10.1038/nature08040
17 Zhu, S. *et al.* BMI1 is directly regulated by androgen receptor to promote castration-resistance in prostate cancer. *Oncogene* **39**, 17-29 (2020). https://doi.org/10.1038/s41388-019-0966-4
18 Zhu, S. *et al.* BMI1 regulates androgen receptor in prostate cancer independently of the polycomb repressive complex 1. *Nat Commun* **9**, 500 (2018). https://doi.org/10.1038/s41467-018-02863-3
19 Voncken, J. W. *et al.* Chromatin-association of the Polycomb group protein BMI1 is cell cycle-regulated and correlates with its phosphorylation status. *Journal of cell science* **112 (Pt 24)**, 4627-4639 (1999).
20 Senthil Kumar, S. *et al.* Diffuse Intrinsic Pontine Glioma Cells Are Vulnerable to Mitotic Abnormalities Associated with BMI-1 Modulation. *Mol Cancer Res* **18**, 1711-1723 (2020). https://doi.org/10.1158/1541-7786.MCR-20-0099
21 Toyoshima, F., Moriguchi, T., Wada, A., Fukuda, M. & Nishida, E. Nuclear export of cyclin B1 and its possible role in the DNA damage-induced G2 checkpoint. *EMBO J* **17**, 2728-2735 (1998). https://doi.org/10.1093/emboj/17.10.2728
22 Clute, P. & Pines, J. Temporal and spatial control of cyclin B1 destruction in metaphase. *Nat Cell Biol* **1**, 82-87 (1999). https://doi.org/10.1038/10049
23 Hagting, A., Jackman, M., Simpson, K. & Pines, J. Translocation of cyclin B1 to the nucleus at prophase requires a phosphorylation-dependent nuclear import signal. *Curr Biol* **9**, 680-689 (1999). https://doi.org/10.1016/s0960-9822(99)80308-x
24 Forbes, D. J., Travesa, A., Nord, M. S. & Bernis, C. Nuclear transport factors: global regulation of mitosis. *Curr Opin Cell Biol* **35**, 78-90 (2015). https://doi.org/10.1016/j.ceb.2015.04.012
25 Weis, K. Regulating access to the genome: nucleocytoplasmic transport throughout the cell cycle. *Cell* **112**, 441-451 (2003). https://doi.org/10.1016/s0092-8674(03)00082-5
26 Hagting, A., Jackman, M., Simpson, K. & Pines, J. Translocation of cyclin B1 to the nucleus at prophase requires a phosphorylation-dependent nuclear import signal. *Current Biology* **9**, 680-689 (1999). https://doi.org/https://doi.org/10.1016/S0960-9822(99)80308-X
27 Xu, D., Farmer, A., Collett, G., Grishin, N. V. & Chook, Y. M. Sequence and structural analyses of nuclear export signals in the NESdb database. *Molecular Biology of the Cell* **23**, 3677-3693 (2012). https://doi.org/10.1091/mbc.e12-01-0046

28 Dong, X. *et al.* Structural basis for leucine-rich nuclear export signal recognition by CRM1. *Nature* **458**, 1136-1141 (2009). https://doi.org/10.1038/nature07975
29 La Cour, T. *et al.* Analysis and prediction of leucine-rich nuclear export signals. *Protein Engineering, Design and Selection* **17**, 527-536 (2004). https://doi.org/10.1093/protein/gzh062
30 Fung, H. Y. J., Fu, S.-C. & Chook, Y. M. Nuclear export receptor CRM1 recognizes diverse conformations in nuclear export signals. *eLife* **6** (2017). https://doi.org/10.7554/elife.23961
31 Fung, H. Y. J., Fu, S.-C., Brautigam, C. A. & Chook, Y. M. Structural determinants of nuclear export signal orientation in binding to exportin CRM1. *eLife* **4** (2015). https://doi.org/10.7554/elife.10034
32 Baumhardt, J. M. *et al.* Recognition of nuclear export signals by CRM1 carrying the oncogenic E571K mutation. *Molecular Biology of the Cell* **31**, 1879-1891 (2020). https://doi.org/10.1091/mbc.e20-04-0233
33 Kumar, S. S. *et al.* BMI-1 is a potential therapeutic target in diffuse intrinsic pontine glioma. *Oncotarget* **8**, 62962-62975 (2017). https://doi.org/10.18632/oncotarget.18002
34 Voncken, J. W. *et al.* MAPKAP kinase 3pK phosphorylates and regulates chromatin association of the polycomb group protein Bmi1. *J Biol Chem* **280**, 5178-5187 (2005). https://doi.org/10.1074/jbc.M407155200
35 Voncken, J. W. *et al.* Chromatin-association of the Polycomb group protein BMI1 is cell cycle-regulated and correlates with its phosphorylation status. *J Cell Sci* **112 (Pt 24)**, 4627-4639 (1999). https://doi.org/10.1242/jcs.112.24.4627
36 Banerjee Mustafi, S. *et al.* Mitochondrial BMI1 maintains bioenergetic homeostasis in cells. *FASEB J* **30**, 4042-4055 (2016). https://doi.org/10.1096/fj.201600321R
37 Liu, J. *et al.* Bmi1 regulates mitochondrial function and the DNA damage response pathway. *Nature* **459**, 387-392 (2009). https://doi.org/10.1038/nature08040
38 Kim, M. J. *et al.* Abstract 5517: PTC596-induced Bmi1 hyper-phosphorylation via Cdk1/2 activation resulting in tumor stem cell depletion. *Cancer Research* **74**, 5517-5517 (2014). https://doi.org/10.1158/1538-7445.Am2014-5517
39 Fornerod, M., Ohno, M., Yoshida, M. & Mattaj, I. W. CRM1 is an export receptor for leucine-rich nuclear export signals. *Cell* **90**, 1051-1060 (1997). https://doi.org/10.1016/s0092-8674(00)80371-2
40 Arnaoutov, A. *et al.* Crm1 is a mitotic effector of Ran-GTP in somatic cells. *Nat Cell Biol* **7**, 626-632 (2005). https://doi.org/10.1038/ncb1263
41 Suzuki, K., Bose, P., Leong-Quong, R. Y., Fujita, D. J. & Riabowol, K. REAP: A two minute cell fractionation method. *BMC Research Notes* **3**, 294 (2010). https://doi.org/10.1186/1756-0500-3-294

Umaru, Figure 1

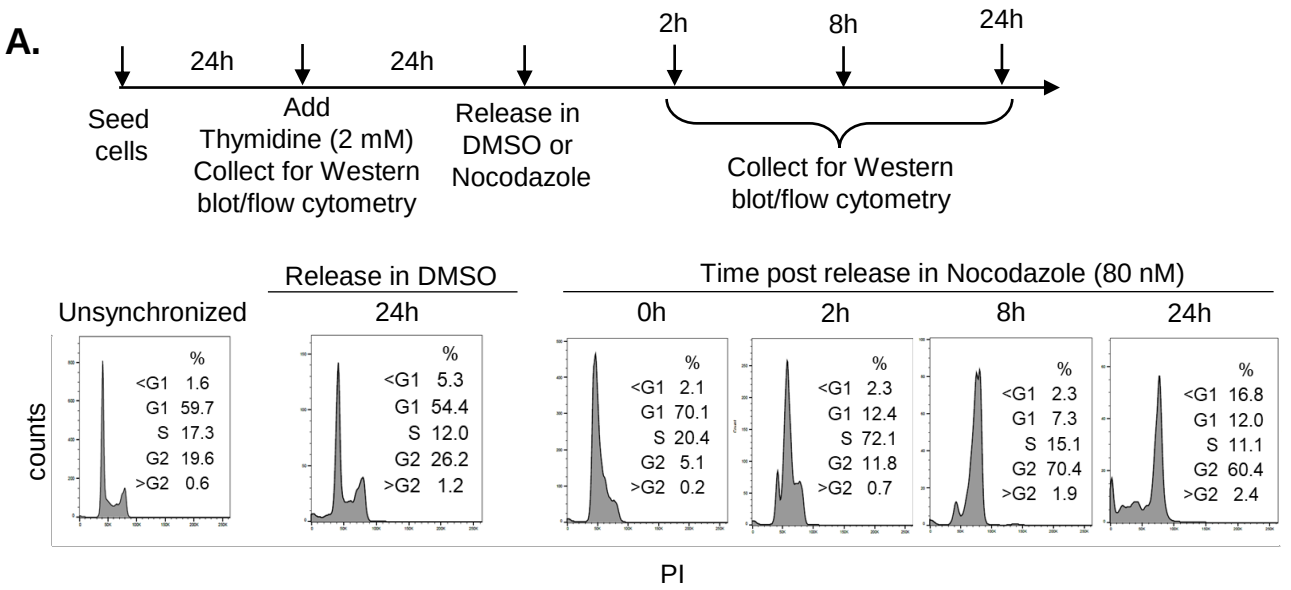

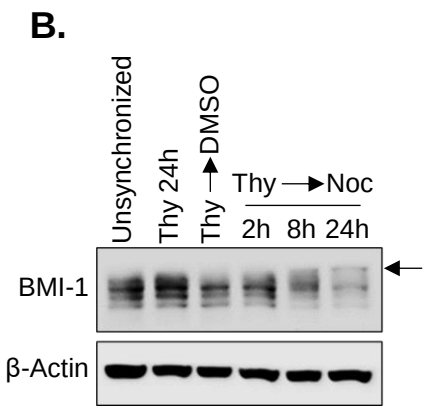

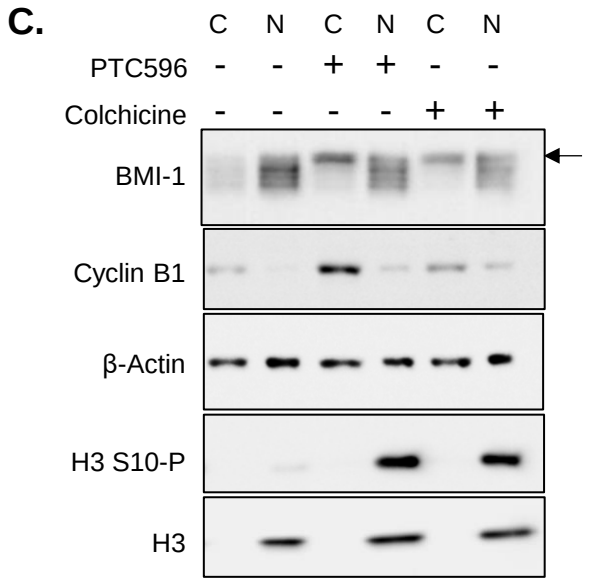

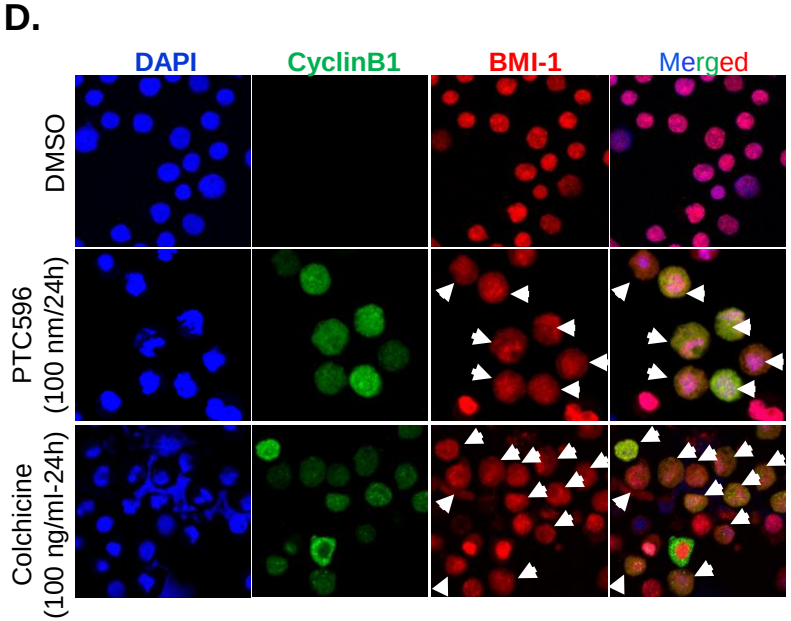

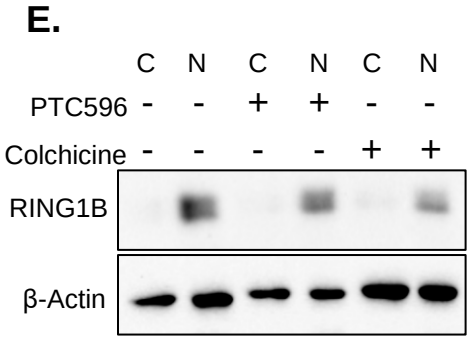

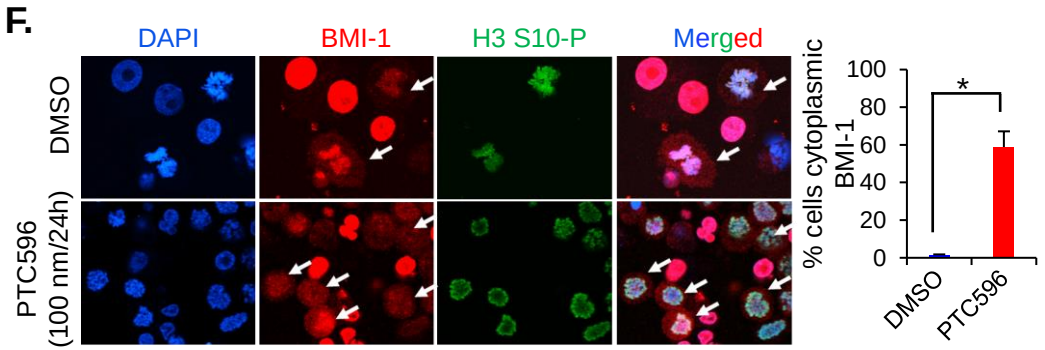

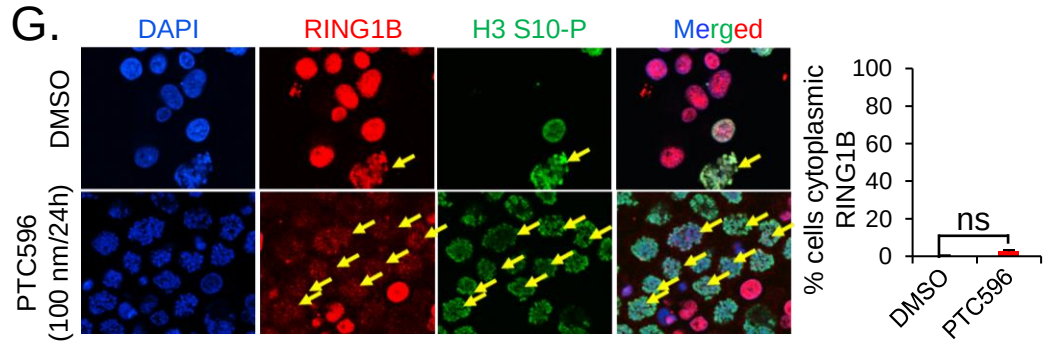

Umaru, Figure 2

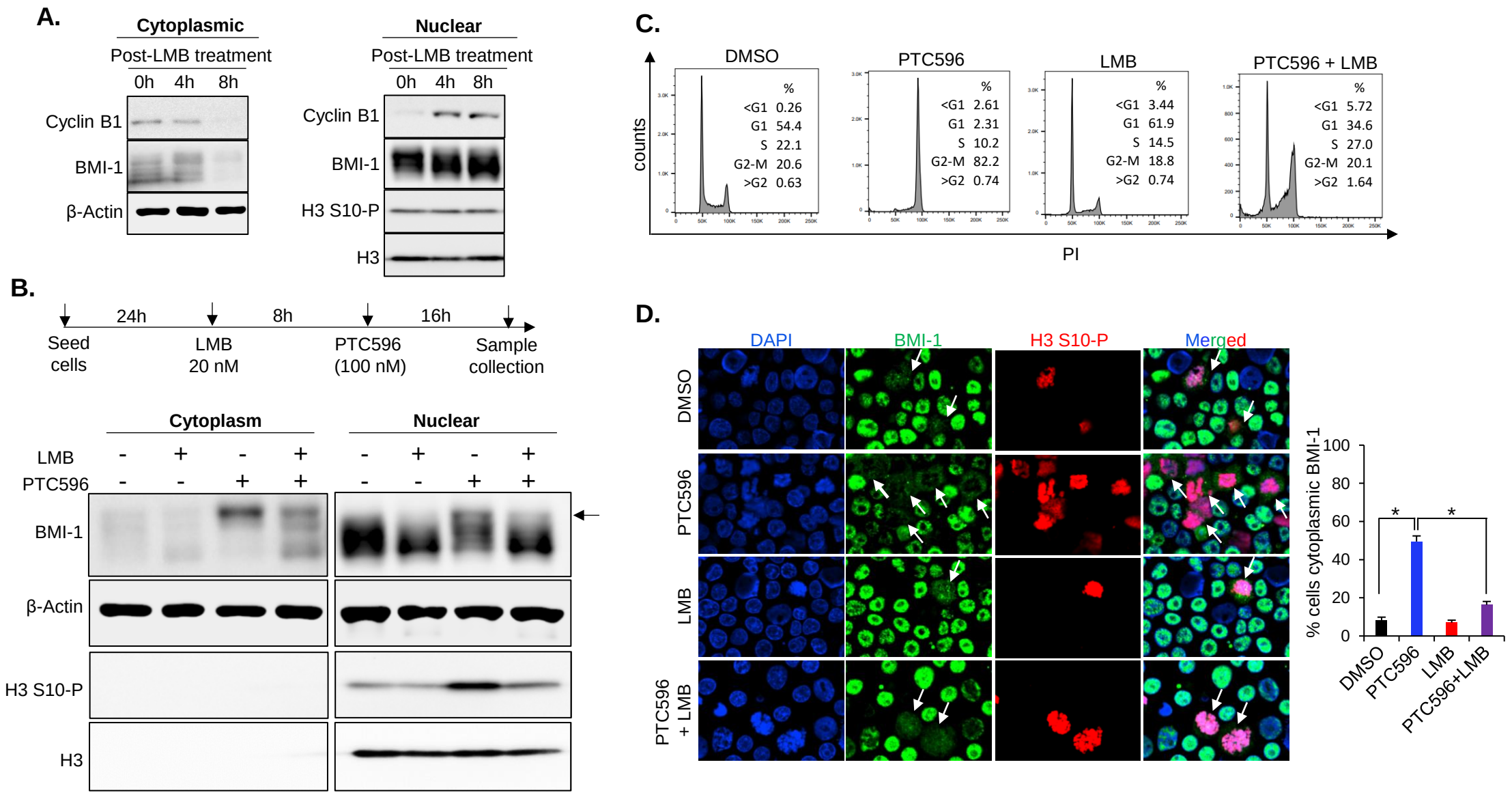

Umaru, Figure 3

A.

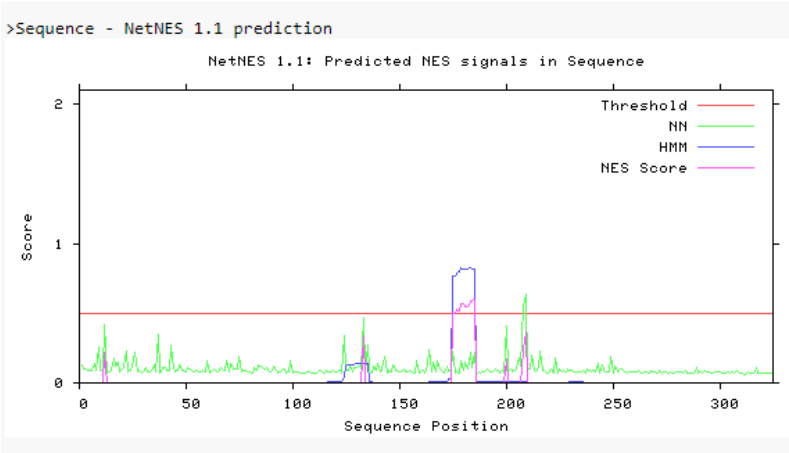

B.

BMI-1-NES Drosophila	L	K	R	F	L	C	S	K	Y	N	I
BMI-1-NES Xenopus	L	R	K	F	L	R	S	K	M	D	I
BMI-1-NES Mus	L	R	K	F	L	R	S	K	M	D	I
BMI-1-NES Homo	L	R	K	F	L	R	S	K	M	D	I
TERT-NES Homo	M	R	R	K	L	F	G	V	L	R	L
SNUPN-NES Homo	L	S	Q	A	L	A	S	S	F	S	V
NES Consensus (Class 1C)	ϕ	X	X	X	ϕ	X	X	X	ϕ	X	ϕ

Φ = L, I, M, V, F
X = an amino acid

C.

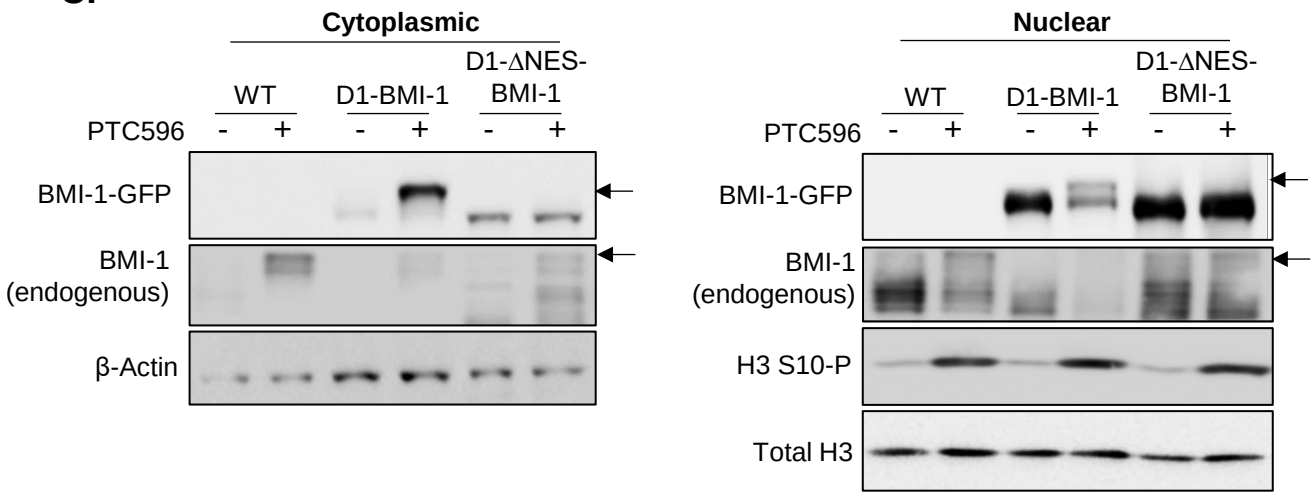

D.

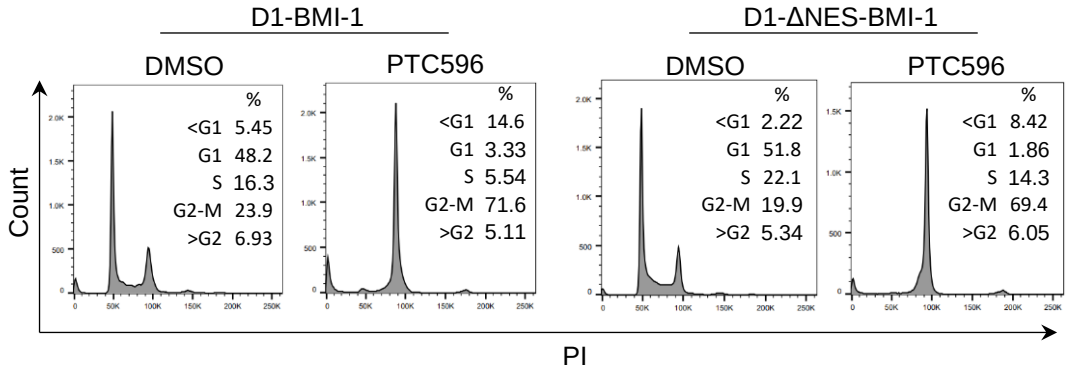

Umaru, Figure S1

A.

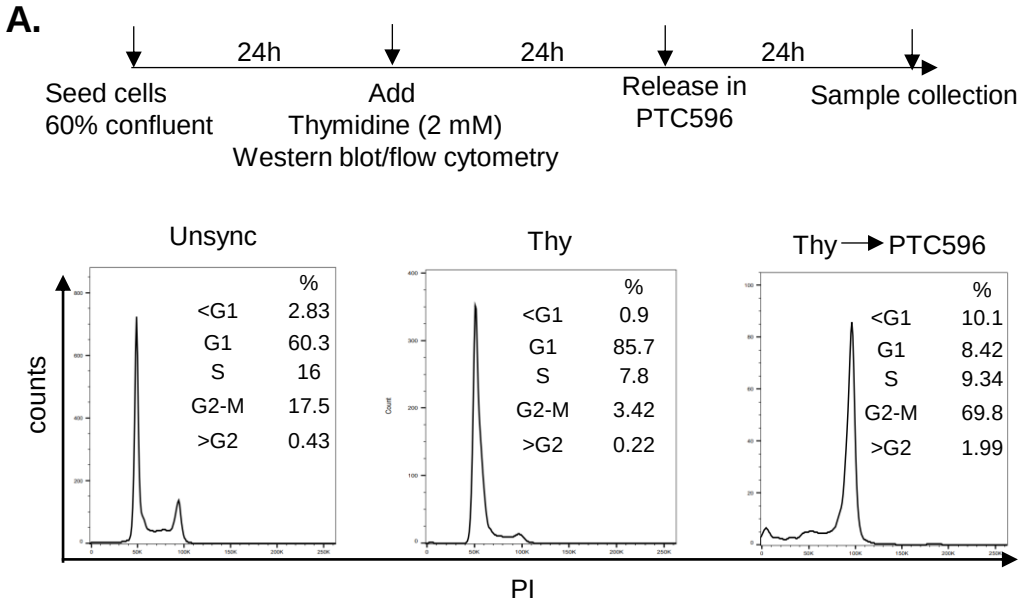

B.

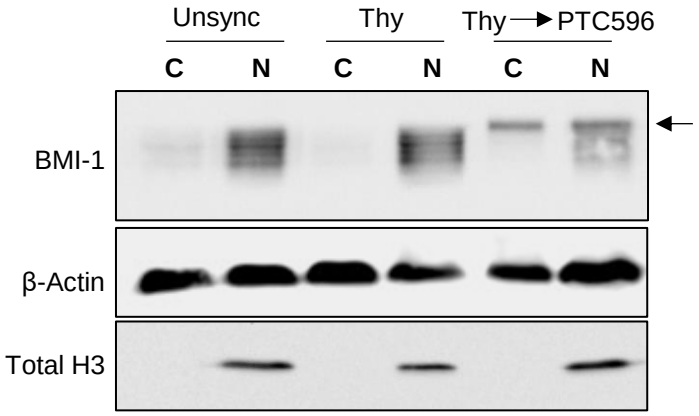

C.

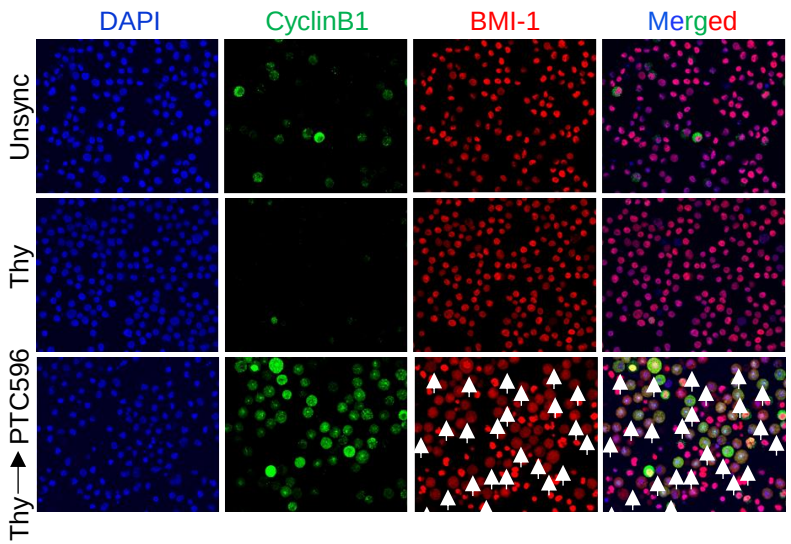

D.

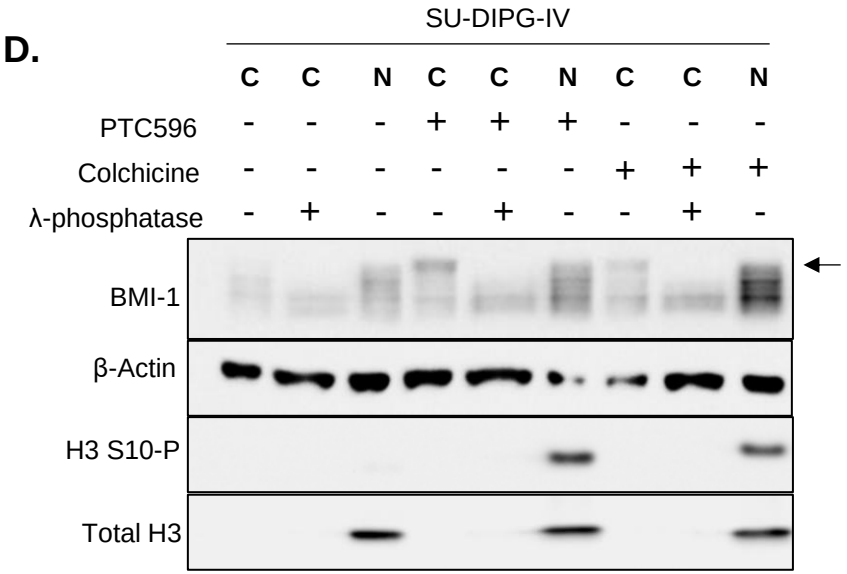

Figure S1.

(A) Scheme representing the cell synchronization studies with thymidine block and release in PTC596, along with collection timepoints for cell cycle analysis (with indicated percentage of cells).

(B) Immunoblot analysis of BMI-1 from cytoplasmic (C) and nuclear (N) fractions. Actin and total H3 served as loading control. Arrow indicates phosphorylated BMI-1.

(C) Representative immunofluorescence images of Cyclin B1 (green) and BMI-1(red). DAPI (blue) represent nuclei. White arrows indicate the cells with cytoplasmic localization of BMI-1. CCHMC-DIPG-1 cells were used for the above experiments.

(D) Immunoblot analysis of BMI-1 from cytoplasmic (C) and nuclear (N) fractions of SU-DIPG-IV cells treated with PTC596 (100 nM for 24h) or colchicine (100 ng/mL for 24 h). Cytoplasmic fractions were further treated with or without λ-phosphatase. Arrow indicated phosphorylated BMI-1.

Umaru, Figure S2

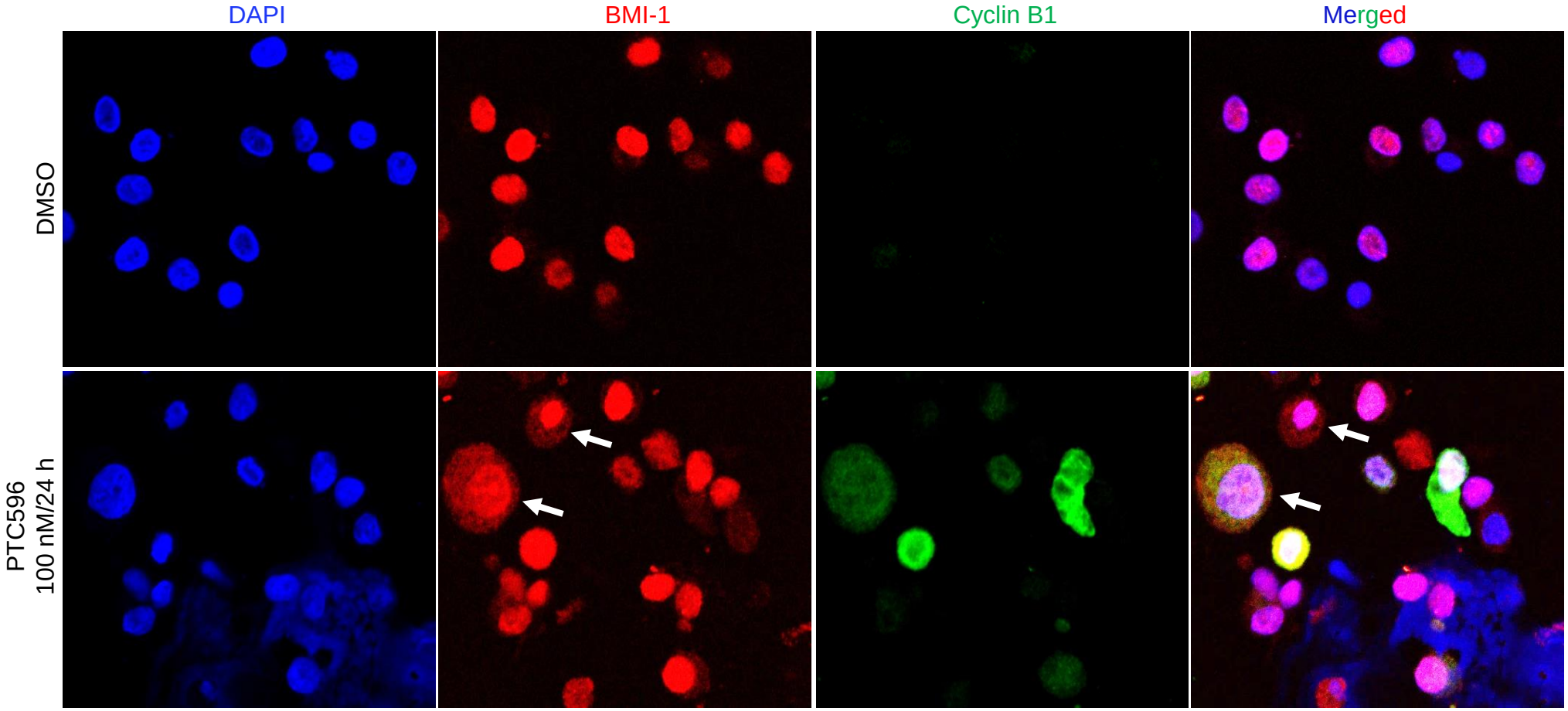

Figure S2.

Representative immunofluorescence images of BMI-1 (red) and Cyclin B1(green). White arrows indicate cells with both cytoplasmic and nuclear BMI-1. DAPI (blue) represents nuclei.

Umaru, Figure S3

A.

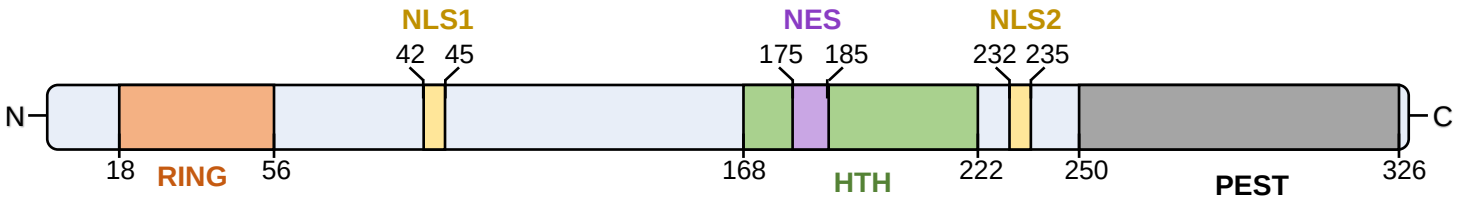

B.

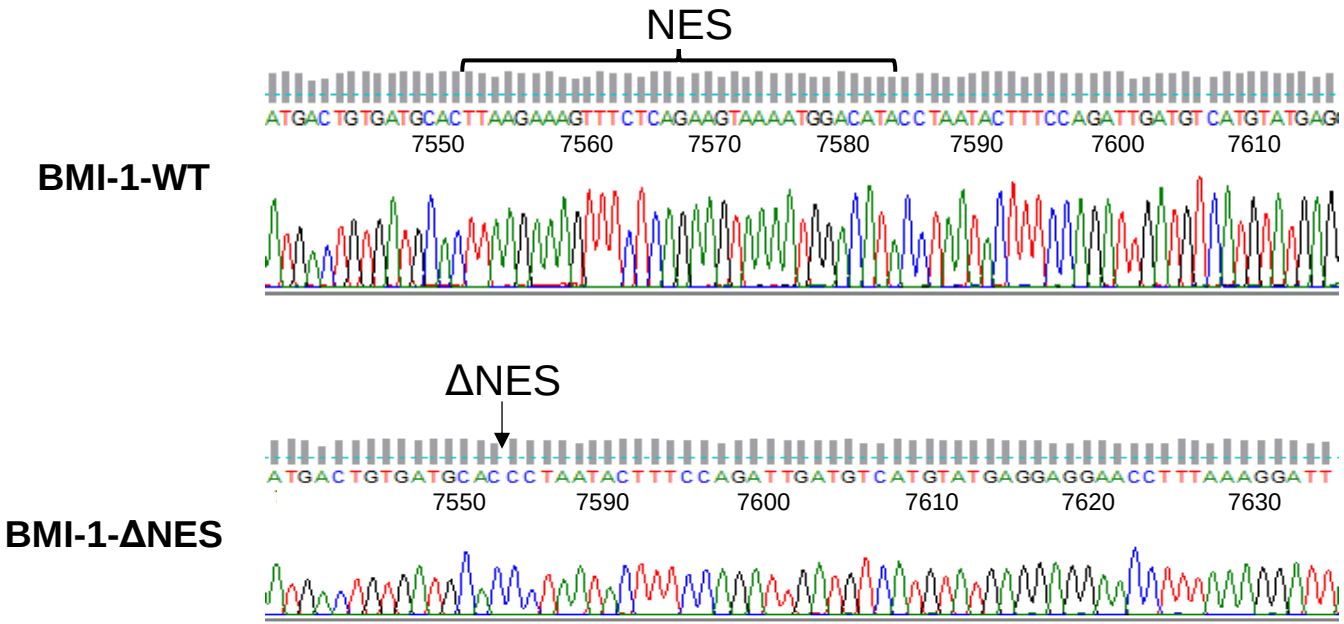

Figure S3.

(A) Schematic illustration of different domains of the BMI-1 protein structure. The newly identified NES domain within the HTH domain is indicated

(B) Genomic DNA extracted from D1-BMI-1 and D1-ΔNES-BMI-1 cells were PCR amplified, and Sanger sequenced to confirm deletion of the NES sequence. The numbers indicate the nucleotide position in *BMI-1* gene.